ARCHIVES
of
FOUNDRY ENGINEERING

ISSN (2299-2944)
Volume 2025
Issue 4/2025

124 – 132

17/4

10.24425/afe.2025.155389

Published quarterly as the organ of the Foundry Commission of the Polish Academy of Sciences

The Effect of Changes in Degassing Parameters on Gasification and Crystallization of EN AC-46000 Alloy

T. Szymczak *, B.P. Pisarek, P. Just, R. Kaczorowski, G. Gumienny, R. Władysiak, C. Rapiejko
Department of Materials Engineering and Production Systems, Lodz University of Technology, Poland
* Corresponding author: E-mail address: tomasz.szymczak@p.lodz.pl

Received 02.09.25; accepted in revised form 06.10.25; available online 31.12.2025

Abstract

The paper presents research on the influence of degassing process parameters on the crystallization and gasification of EN AC-46000 alloy (designation according to chemical composition – AlSi9Cu3(Fe)). After melting, the alloy was degassed using Ecosal Al113.S solid refiner and by blowing with an inert gas: nitrogen or argon. Various solid degasser contents and various nitrogen and argon blowing times were used. Thermal and derivative analysis (TDA) were used to study the crystallization process of Al-Si alloy. The density index as well as hydrogen content in the liquid alloy were determined. Using Alu Speed Tester, it was demonstrated that the lowest density index and hydrogen content were obtained in the alloy degassed with the use of Ecosal at a concentration of 1% and then blown with argon for 15 minutes. It has been shown that increasing the efficiency of the degassing process results in prolonging the crystallization time of the tested alloy, and in particular, the crystallization time of $\alpha_{Al} + \beta(Si)$ binary eutectic. The justification given was the probable removal of small solid particles from the liquid metal, which could form the basis for heterogeneous nucleation of the Al-Si alloy component phases during degassing.

Keywords: Degassing, Crystallization process, Gasification, EN AC-46000 Alloy, Die casting

1. Introduction

Degassing is a process carried out on molten metal to purify it of gases and solid impurities in the form of oxides, borides, nitrides, or spinels, as well as harmful elements such as Li, Be, and Ca, and excess Na, Sr, or Mg [1-5]. Solid or gaseous degassers are used to remove gases from Al-Si alloys. Sodium fluoride and calcium, potassium or magnesium chlorides are most used as solid degassing agents for Al-Si alloys. These are chemical compounds that bind impurities in liquid metal. Inert gases such as nitrogen, argon, chlorine, or mixtures thereof are used as gas degassers. Blowing aluminum alloys with inert gases causes hydrogen to be absorbed by gas bubbles flowing through the liquid alloy. Ultrasound, infrasound, variable electromagnetic fields, vacuum, and elevated pressure are also used for degassing [5-14].

High hydrogen concentrations in Al-Si alloys result in porosity in castings, which is particularly prevalent in high pressure die castings. High pressure exerted on the liquid alloy in the pressure mold causes many hydrogen bubbles to be released from it, which remain in the microstructure after crystallization is complete. The use of alloy degassing for die casting can significantly reduce the degree of gasification and, consequently, porosity in the casting.

In numerous studies, authors show that the degassing process significantly contributes to reducing impurities in aluminum alloys, particularly their gas content. In turn, reducing the gas content in

liquid Al alloys results in reduced porosity in castings, and consequently increases their tightness and mechanical properties [15-19].

The harmful effects of contamination in Al-Si alloys, particularly excessive hydrogen content, are well known and widely documented [20]. Much attention in the industry literature is devoted to the harmful effect of excessive amounts of impurities, including H_2, on the decomposition and porosity of Al-Si alloy castings and, consequently, on the reduction of their mechanical properties. Much less attention is paid to the influence of degassing on the crystallization process of Al-Si alloys.

In view of the above, this study examined the effect of selected technological factors in the degassing process using both solid and gas degassers on the level of gasification and the crystallization process of EN AC-46000 alloy. The tested technological parameters of refining were the amount of solid degasser (Ecosal) and the time of blowing the liquid alloy with nitrogen (N_2) or argon (Ar). The level of the alloy gasification was identified by determining the so-called density index (DI) and hydrogen (H_2) content. The alloy crystallization process was characterized using characteristic point coordinates determined by Thermal and Derivative Analysis (TDA).

2. Methodology

2.1. Chemical composition and alloy preparation

EN AC-46000 alloy was used as the initial alloy for the tests. Its chemical composition range, in accordance with PN-EN 1706 [21], is presented in Table 1.

Table 1.
Chemical composition range of EN AC-46000 alloy used for testing according to PN-EN 1706

Si	Cu	Zn	Fe	Mg	Mn	Ni	Pb	Ti	Sn	Cr	rest	
											individ.	all
8.0–11.0	2.0–4.0	max. 1.2	max. 1.3	0.05–0.55	max. 0.55	max. 0.55	max. 0.35	max. 0.25	max. 0.15	max. 0.15	max. 0.05	max. 0.25

Preliminary studies have shown that Si, Cu, and Mg have the greatest influence on the mechanical properties of the alloy among its constituent elements. It has also been shown that to obtain the best strength properties within the standardized chemical composition of the alloy, the content of these elements should be limited to the following ranges: 9.0–10.0% Si; 2.0–2.5% Cu and 0.3–0.4% Mg. For the purposes of this study, it was assumed that the content of Si, Cu, and Mg should fall within the narrow ranges specified above, while the content of other constituent elements should fall within the ranges specified in PN-EN 1706 (Tab. 1). The full chemical composition of the alloy used for the tests is presented in Table 2. The chemical composition of the alloys was determined using a stationary metal analyzer SPECTROMAXx (SPECTRO Analytical Instruments GmbH, Kleve, Germany).

Table 2.
Chemical composition range of EN AC-46000 alloy used for the tests

Si	Cu	Zn	Fe	Mg	Mn	Ni	Ti	Cr	Al
9.39–9.71	2.17–2.44	0.93–1.19	0.91–0.97	0.29–0.37	0.22–0.23	0.11–0.12	0.030–0.050	0.020–0.032	rest

The variable parameters of the argon and nitrogen degassing process were the time of blowing the liquid metal with these gases while maintaining a constant gas volume flow rate. When using a solid degasser, the variable parameter was the percentage of Ecosal in the alloy. The amount of solid degasser as well as the degassing time for Ar or N_2 were applied according to the planned two-level experiment, which is characterized in Figure 1 and Table 3.

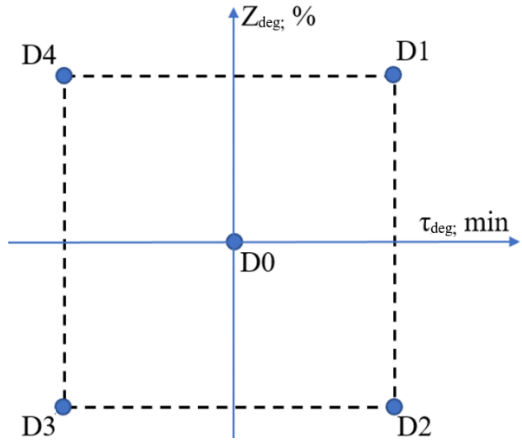

Fig. 1. Experiment plan diagram

where:
Z_{deg}, % – content of solid degasser (Ecosal) in the alloy,
τ_{deg}, min – time for blowing through the liquid alloy with an inert gas: nitrogen (N_2) or argon (Ar).

Table 3.
Degassing parameters for individual melts

Melt number	Z_{deg} (Ecosal); %	τ_{deg} (Ar or N_2); min
D0	0.5	7.5
D1	1.0	15.0
D2	0.0	15.0
D3	0.0	0.0
D4	1.0	0.0

The data presented in Fig. 1 and Table 3 show that the D3 melt refers to an alloy that has not been degassed. In the case of D4 smelting, only Ecosal in an amount of Z_{deg} = 1%was used for degassing, while in the case of D2 smelting, only any tested inert

gas was used (blowing time τ_{deg} = 15 min). The central point D0 and point D1 represent melts where degassing with Ecosal was performed, followed by gas degassing. The Z_{deg} and τ_{deg} values for these melts are presented in Fig. 1b.

The alloy was melted in an ELKON PI 30 induction furnace (ELKON LLC, Rybnik, Poland) in an AC20 crucible made of SiC with a capacity of 7 kg of Al alloy. The metal charge as EN AC-46000 alloy ingots was melted and superheated to a temperature of 750 ± 10°C. To obtain the desired Si, Cu, and Mg content in individual melts, Si or Al and Cu were added to the bath in the form of technically pure metals, while magnesium was added as AZ91 alloy. After dissolving the alloying additives in the liquid alloy, degassing with Ecosal Al113S solid degasser was carried out, followed by gas degassing with nitrogen or argon.

Gas degassing (with N_2 or Ar) was carried out using a steel lance inserted into the bottom of the AC20 crucible. To reduce the hydrogen content, the melt was purged with gases for a specified period. After blowing was completed, the slag was removed from the surface of the melt, and the temperature was stabilized at the selected level. The gas degassing process is shown in Figure 2.

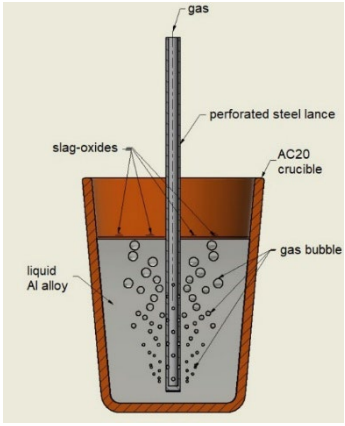

Fig. 2. Schematic diagram of gas degassing (with N_2 or Ar) using a perforated steel lance [own study]

2.2. Test castings production

After degassing, the temperature of the liquid metal was lowered to 700±10 °C and the crystallization process was examined using Thermal and Derivative Analysis (TDA) and its gasification.

2.3. Thermal and derivative analysis

The thermal and derivative analysis (TDA) characteristics were recorded at an alloy quality control station equipped with a computer, Crystaldigraph, stand, and TDA probe. The probe, made as a shell sand mold, is shown in Figure 3.

A PtRh10-Pt thermocouple was used to record the temperature, which was inserted into the quartz tube of the TDA probe (Fig. 3). A numerical filter of derivative 15 was used to present the curves in the paper.

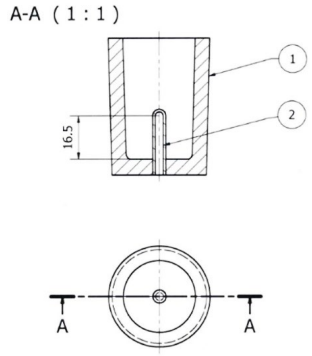

Fig. 3. TDA probe: 1) shell mold, 2) quartz tube closed on one side [own study]

The recorded TDA characteristics consist of a temperature change curve $t=f(\tau)$ and a curve of the kinetics of thermal crystallization processes (the so-called derivative curve) $dt/d\tau=f'(\tau)$. The derivative curve $dt/d\tau=f'(\tau)$ was determined based on $t=f(\tau)$ curve. On the derivative curve, characteristic points were determined: local extrema (minima and maxima) and values $dt/d\tau=0$. The characteristic points of TDA curves can therefore be determined by specifying the values of the following variables: temperature "t", time "τ" from the start of recording, and the value of the first derivative "K= $dt/d\tau$".

2.4. Alloy gasification analysis

The DI density index and hydrogen content were determined using the Alu Speed Tester (FMA, Schaan, Liechtenstein) with an FMA Balance scale.

2.4.1. Density index determination

The alloy density index (DI) was determined based on density measurements of specimens cast into metal molds on the Alu Speed Tester. The first specimen solidified at ambient temperature and pressure, while the second solidified at a reduced pressure of 80 mbar. The density of the specimens after cooling to ambient temperature, D_{atm} for the first specimen and D_{80mbar} for the second specimen, was measured on a dedicated FMA index scale, while the density index was automatically calculated using the Archimedes Principle function.

Based on the determined specimens' densities, the density index DI in % can be calculated using formula (1):

$$DI=(D_{atm}-D_{80mbar})/D_{atm}\cdot 100,\ \% \quad (1)$$

where:

D_{atm} – density of the alloy specimen solidifying at atmospheric pressure, g/cm^3,

D_{80mbar} – density of the alloy specimen solidifying at reduced pressure to 80 mbar, g/cm^3.

2.4.2. Measurement of hydrogen content in alloy

The measurement of hydrogen content in alloy is based on the principle of the first gas bubble according to Y. Dardel. When the

ambient pressure is lower than or equal to the partial pressure in the molten metal, the gas escapes from it due to the difference in density. This has been observed in the form of bubbles on the surface of the liquid metal.

The concentration of hydrogen C_H is calculated based on the partial pressure of hydrogen P_H, the temperature of the liquid alloy T, and the constants (A, B) for the alloying elements such as Cu, Si, Mg, Mn. The hydrogen concentration H_2, in accordance with "Sieverts' rule", was determined using formula (2):

$$\log H_2 = 0{,}5 \cdot \log P_H - A/T + B \quad (2)$$

where:

H_2 – concentration of dissolved hydrogen in aluminum alloy, $cm^3/100$ g,

P_H – partial pressure of hydrogen, mbar,

T – liquid alloy temperature, K,

A, B – empirical constants dependent on alloy composition.

2.5. Microstructural tests

Metallographic sections were made on specimens taken from the TDA probe, and its surface was etched with a 2% aqueous solution of HF acid. The prepared specimens were observed, and microstructure photographs were taken using a Nikon Eclipse MA200 metallographic microscope (Nikon Metrology Inc.), equipped with Nikon DS-Fi 1 digital camera. The photographs were recorded using NIS-Elements Advanced Research digital image analysis software. The microstructure examination was each time performed in the same place of the test casting, in the area located in the axis of rotation of the casting just above the quartz tube that constituted the shield for the thermocouple (Fig. 3).

3. Results

3.1. Alloy gasification analysis

Tables 4 and 5 present the measurement results of the density index and hydrogen content in the tested castings.

Table 4.
Density index DI and hydrogen content for the test series using degassing with argon

Melt number	Z_{deg} (Ecosal); %	τ_{deg} (Ar); min	DI; %	H_2 content; $cm^3/100g$
D0	0.5	7.5	0.39	0.09
D1	1.0	15	0.14	0.04
D2	0.0	15	0.35	0.09
D3	0.0	0.0	2.18	0.16
D4	1.0	0.0	1.17	0.13

Table 5.
Density index DI and hydrogen content for the test series using degassing with nitrogen

Melt number	Z_{deg} (Ecosal); %	τ_{deg} (N_2); min	DI; %	H_2 content; $cm^3/100g$
D0	0.5	7.5	0.59	0.10
D1	1.0	15	0.26	0.07
D2	0.0	15	1.00	0.13
D3	0.0	0.0	2.18	0.16
D4	1.0	0.0	1.17	0.13

The research showed that the highest gas content was found in the undegassed alloy, i.e. D3 melt common to both research series. Then the alloy is characterized by the highest values of DI = 2.18% and H_2 = 0.16 $cm^3/100g$. Degassing only with Ecosal in the amount of Z_{deg} = 1% (melt D4, also common to both research series) resulted in a reduction of the alloy gasification, the values of the tested alloy quality parameters decreased to DI = 1.17% and H_2 = 0.13 $cm^3/100g$. Also, the use of only gas (D2 melts), regardless of its type, resulted in a reduction in the gas content. In the case of blowing with argon at τ_{deg} = 15 min, DI = 0.35% and H_2 content = 0.09 $cm^3/100$ g were obtained, while the same time of blowing with nitrogen allowed to obtain DI = 1.00% and H_2 content = 0.13 $cm^3/100$ g. Achieving a similar or better degassing effect was possible thanks to the combined degassing, first with Ecosal and then with inert gas (Ar or N_2). The use of 0.5% Ecosal and subsequent argon blowing for 7.5 minutes (D0 melts) resulted in a melt characterized by DI = 0.39% and H_2 = 0.09 $cm^3/100$ g. For the same degassing parameters (Z_{deg} and τ_{deg}), but using nitrogen as a gas degasser, an alloy with DI = 0.59% and H_2 = 0.10 $cm^3/100$ g was obtained. The best degassing effect was achieved for D1 melts, i.e. for the highest amount of solid degasser 1% and the longest gas blowing time 15 min, regardless of the type of degassing gas. The use of above-mentioned degassing parameters with argon resulted in an alloy with DI = 0.14% and H_2 = 0.04 $cm^3/100$ g. On the other hand, the use of nitrogen with the same degassing parameters resulted in an alloy with DI = 0.26% and H_2 = 0.09 $cm^3/100$ g.

3.2. Study of crystallization parameters

Figure 4 shows example TDA curves of undegassed EN AC-46000 alloy.

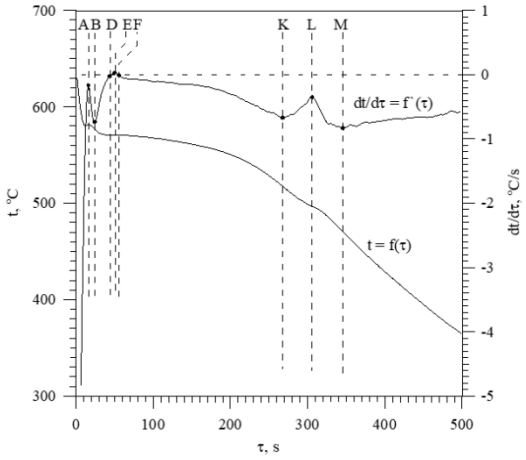

Fig. 4. Example TDA curves for undegassed EN AC-46000 alloy

Fig. 4 shows two curves: the melt temperature change curve t = f(τ) and the derivative curve dt/dτ = f`(τ).

There are three thermal effects on the derivative curve resulting from changes occurring during the cooling and solidification. The thermal effect described by points AB results from the crystallization of primary dendrites of α_{Al} solid solution. Point A denotes the maximum thermal effect caused by the crystallization of the α_{Al} solid solution, i.e., the moment of the most intense release of latent heat of crystallization, while point B denotes the end of crystallization of this phase and the beginning of the next phase crystallization in the described system. It is described by BDEFK thermal effect $\alpha_{Al} + \beta(Si)$ eutectic mixture. Points D and F represent so-called zero points, where dt/dτ = 0; and when transferred to the t=f(τ) curve, these are the points determining the minimum (point D) and maximum (point F) temperatures in temperature recalescence during the crystallization of $\alpha_{Al}+\beta(Si)$ eutectic mixture. Point E marks the maximum thermal effect of eutectic mixture crystallization. At point K, the crystallization of $\alpha_{Al} + \beta(Si)$ binary eutectic terminates and the crystallization of another, more complex eutectic mixture begins. It contains not only α_{Al} and β(Si) solid solutions but also intermetallic phases rich in Cu and Mg. On the differential curve, this is visible as KLM thermal effect. Point L represents the maximum thermal effect from the crystallization of this eutectic, while at point M the crystallization of this eutectic and the entire alloy terminates. The description of the crystallization process of multicomponent hypereutectic Al-Si alloy and the types of phases occurring in it are widely documented in the industry literature [22-24].

A broader overview of TDA curves for a series of tests using argon degassing is presented in Figure 5.

Regarding the complete set of melts defined in the experimental design (Fig. 1), the summary presented in Fig. 5 curves for melt D0 (the central point of the experimental design) are missing. At this point, as at point D1, combined degassing with Ecosal and argon was performed. The curves in these two smeltings were similar. Curves for D1 melting are presented, in which the alloy was refined using the maximum tested values of Z_{deg} and τ_{deg} parameters. Tables 6-8 present the coordinates of characteristic points of all TDA curves for alloys after argon degassing. These are, respectively, the values of time from the start of recording "τ", temperature "t" and the first derivative of temperature calculated with respect to time "K= dt/dτ".

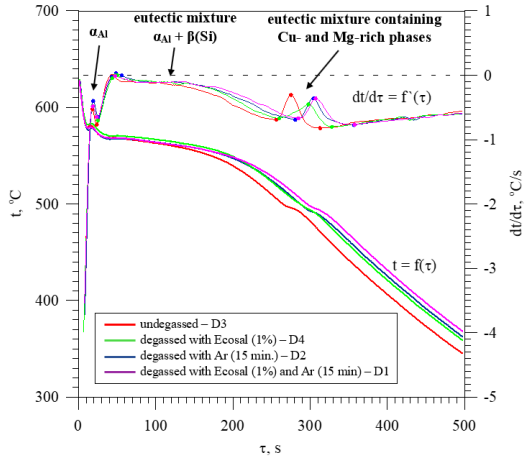

Fig. 5. Example TDA curves for EN AC-46000 alloy recorded in a series of tests using Ecosal and argon (Ar) degassing process

Table 6.
Time "τ" from the start of recording at characteristic points of TDA curves of the tested Al-Si alloy degassed with Ecosal and argon (Ar)

Melt number	τ, s							
	τA	τB	τD	τE	τF	τK	τL	τM
D0	18.5	26.2	43.5	49.9	55.6	267.5	293.7	342.4
D1	17.3	25.0	-	48.0	-	290.0	309.2	359.1
D2	18.4	26.1	44.6	48.5	58.1	283.4	305.8	355.7
D3	15.3	23.0	38.4	41.6	44.1	254.0	274.5	310.4
D4	17.6	25.6	45.1	51.2	55.0	263.6	303.3	337.2

Table 7.
Temperature "t" at the characteristic points of the TDA curves of tested Al-Si alloy degassed with Ecosal and argon (Ar)

Melt number	t, °C							
	tA	tB	tD	tE	tF	tK	tL	tM
D0	582.2	576.9	569.0	569.2	569.3	508.4	493.1	460.8
D1	579.6	575.0	-	568.3	-	505.4	495.4	463.3
D2	578.3	573.9	567.1	567.2	567.6	504.1	491.7	459.1
D3	581.1	575.0	568.3	568.6	568.7	507.2	496.2	473.6
D4	582.4	577.4	570.4	570.6	570.9	518.2	495.8	473.7

Table 8.
First derivative "K=dt/dτ" at the characteristic points of TDA curves of the tested Al-Si alloy degassed with Ecosal and argon (Ar)

Melt number	K, °C/s							
	KA	KB	KD	KE	KF	KK	KL	KM
D0	-0.23	-0.88	0.00	0.01	0.00	-0.68	-0.35	-0.78
D1	-0.24	-0.79	-	0.00	-	-0.67	-0.33	-0.77
D2	-0.11	-0.77	0.00	0.04	0.00	-0.70	-0.32	-0.78
D3	-0.18	-0.93	0.00	0.02	0.00	-0.70	-0.27	-0.83
D4	-0.19	-0.78	0.00	0.03	0.00	-0.68	-0.39	-0.83

The TDA curves shown in Fig. 5 and the data in Table 6 indicate that, regardless of the degassing variant, the crystallization process takes longer than that of the undegassed alloy. The time

difference between points A and B, which mark the crystallization of α_{Al} solid solution dendrites for undegassed alloy (melt D3), is τB – τA = 7.7 s. For the other melts in this test, the differences between τB and τA are similar and range from 7.7s to 8.0s. Significantly greater differences in time occurred within the crystallization of eutectic mixtures in the alloy under study. The crystallization of α_{Al} + β(Si) binary eutectic mixture occurs during the time "τK - τB", while the crystallization of the complex eutectic mixture containing Cu- and Mg-rich intermetallic phases occurs during the time "τM – τK". The shortest eutectic crystallization time τM – τK = 56.4 s was for undegassed alloy (melt D3). In the case of degassed alloys, the crystallization time "τM – τK" increased and, for all cases of degassing process considered, ranged from 69.1 s to 74.9 s. The most systematic differences in crystallization time were obtained in the case of the phase with the longest crystallization time, i.e., binary eutectic mixture. These differences are presented in Figure 6.

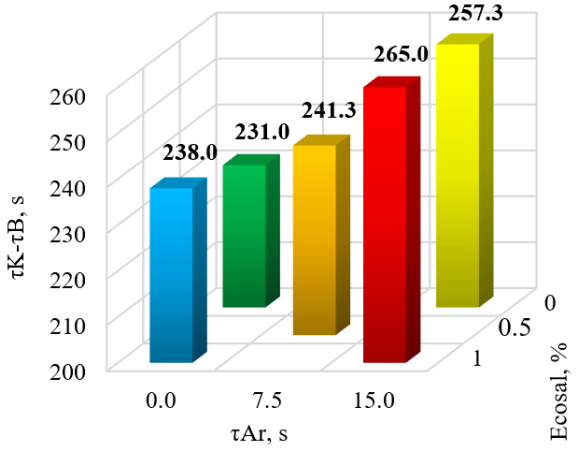

Fig. 6. Crystallization times "τK – τB" of α_{Al} + β(Si) binary eutectic mixture calculated based on characteristic points of TDA curves for Ar-degassed alloys

The data presented shows that, as it was in case of ternary eutectic mixture, the shortest crystallization process of binary eutectic mixture was for undegassed alloy, where τK – τB = 231 s. The use of Ecosal alone (Z_{deg}= 1%) prolonged the eutectic mixture crystallization to 238 s. Performing only gas degassing, i.e., blowing argon for 15 minutes, resulted in prolonging the crystallization of the binary eutectic mixture to 257.3 s. The use of combined degassing (Z_{deg} = 1% and τ_{deg} = 15 min) extended the process to 265.0 s.

No systematic changes were found in the other coordinates of TDA curves characteristic points, i.e. "t" and "K", caused by changes in the degassing parameters under investigation.

Tables 9-11 show the time from the start of recording "τ", temperatures "t" and the first derivative of temperature with respect to time "K= dt/dτ" for the second series of tests using nitrogen degassing. The course of the TDA curves was like the curves obtained for argon-degassed alloys.

Table 9.
Time "τ" from the start of recording at characteristic points of TDA curves of the tested Al-Si alloy degassed with Ecosal and nitrogen (N_2)

Melt number	τ, s							
	τA	τB	τD	τE	τF	τK	τL	τM
D0	18.1	25.8	43.7	48.2	54.0	276.7	301.0	336.2
D1	16.1	23.2	41.7	44.9	47.5	273.4	289.4	346.4
D2	18.1	27.7	48.2	52.0	55.2	270.3	284.4	315.1
D3	15.3	23.0	38.4	41.6	44.1	254.0	274.5	310.4
D4	17.6	25.6	45.1	51.2	55.0	263.6	303.3	337.2

Table 10.
Temperature "t" at the characteristic points of TDA curves of the tested Al-Si alloy degassed with Ecosal and nitrogen (N_2)

Melt number	t, °C							
	tA	tB	tD	tE	tF	tK	tL	tM
D0	578.9	575.3	569.3	569.7	569.9	507.9	493.8	471.0
D1	581.9	577.0	570.4	570.5	570.7	503.2	494.7	482.5
D2	582.0	576.8	569.6	569.8	569.9	501.8	494.6	474.4
D3	581.1	575.0	568.3	568.6	568.7	507.2	496.2	473.6
D4	582.4	577.4	570.4	570.6	570.9	518.2	495.8	473.7

Table 11.
First derivative "K=dt/dτ" at the characteristic points of TDA curves of the tested Al-Si alloy degassed with Ecosal and nitrogen (N_2)

Melt number	K, °C/s							
	KA	KB	KD	KE	KF	KK	KL	KM
D0	0.07	-0.64	0.00	0.04	0.00	-0.71	-0.33	-0.82
D1	-0.23	-0.80	0.00	0.01	0.00	-0.70	-0.34	-0.80
D2	-0.04	-0.77	0.00	0.02	0.00	-0.75	-0.27	-0.87
D3	-0.18	-0.93	0.00	0.02	0.00	-0.70	-0.27	-0.83
D4	-0.19	-0.78	0.00	0.03	0.00	-0.68	-0.39	-0.83

The data presented in Tables 9-11 show that, also for this series of tests, the smallest differences in crystallization time were obtained for the α_{Al} solid solution. In this case, the minimum value of τB – τA = 7.1 s was obtained for melt D1, while the maximum value of τB – τA = 9.6 s was obtained for melt D2. Greater differences were obtained in the case of the crystallization time "τM – τK". The shortest eutectic crystallization time τM – τK = 44.8 s was for the alloy refined with nitrogen for 15 min (melt D2). This is a shorter time compared to undegassed alloy (D3 melt), where "τM – τK" amounts to 56.4 s. For the remaining degassed alloys, the crystallization time of the complex eutectic mixture "τM – τK" was longer than in the above-mentioned melts and ranged from 59.5 s to 73.6 s. Also, in this series of studies, the largest and systematic differences in crystallization times were obtained for binary eutectic mixture. These differences are shown in Figure 7.

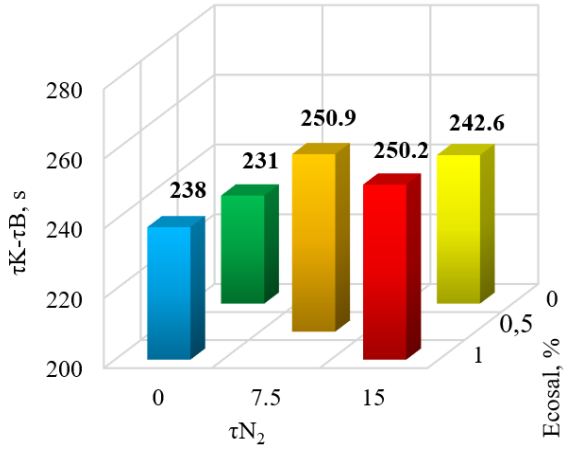

Fig. 7. Crystallization times "τK – τB" of α_{Al} + β(Si) binary eutectic mixture calculated based on characteristic points of TDA curves for N_2-degassed alloys.

The results presented in Fig. 8 show, similarly to argon-degassed alloys, that the crystallization time of the binary eutectic mixture "τK – τB" increased in all degassed melts compared to the undegassed. The longest binary eutectic mixture crystallization time was observed in the case of combined degassing, and thus in melt D0 (Z_{deg} = 0.5% and τ_{deg} = 7.5 min) this time was 250.9 s; and in melt D1 (Z_{deg} = 1.0% and τ_{deg} = 15 min), a similar time 250.2 s was obtained.

Also, in this series of tests, no systematic changes were found in the remaining coordinates of TDA curves characteristic points, i.e., "t" and "K," caused by changes in the degassing parameters.

3.3. Microstructural tests

The microstructure of EN AC-46000 alloy is widely known and extensively described in global literature. According to the literature [22-25], it consists of primary dendrites of α_{Al} solid solution, α_{Al}+β(Si) eutectic mixture, and intermetallic phases, that are part of the complex eutectic mixtures. The most common intermetallic phases in the studied alloy are: Al_2Cu, Mg_2Si, and $Al_{15}(Fe,Mn)_3Si_2$. More complex phases from Al-Cu-Mg-Si (e.g., $Al_8CuMg_8Si_6$ and $Al_5Cu_2Mg_8Si_6$) and Al-Mg-Fe-Si (e.g., $Al_8Mg_3FeSi_6$) systems are also frequently found. The presented description of the microstructure is consistent with the previously presented results of the crystallization studies using TDA method. Figures 8 and 9 show the microstructure of EN AC-46000 alloy without degassing and after degassing with Ecosal (Z_{deg} = 1.0%) and argon (τ_{deg} = 15 min), respectively.

Figures 8 and 9 show that the microstructure of an undegassed alloy contains porosity, whereas a properly conducted degassing process allows it to be almost eliminated.

Fig. 8. Microstructure of undegassed EN AC-46000 alloy from the TDA probe

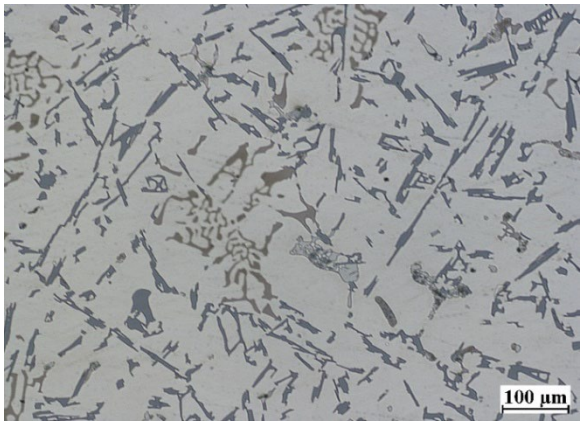

Fig. 9. Microstructure of EN AC-46000 alloy after degassing with Ecosal and argon (Z_{deg} = 1.0%; τ_{deg} = 15 min) from TDA probe

4. Summary

The results presented in this paper indicate that all the degassing variants analyzed produced the desired effect in the form of a reduction in the gas content of the alloy tested. However, the best results are achieved by degassing, which involves initially introducing a solid degasser (Ecosal) into the liquid alloy and then blowing it with an inert gas (Ar or N_2). Among the gases tested, argon causes better degassing. This is confirmed by the results of gasification level tests (DI and H_2 content) conducted both for gas alone and in combination with Ecosal pre-degassing. Of all the variants tested, the best degassing occurred after Ecosal degassing at Z_{deg} = 1.0% and argon blowing at τ_{deg} = 15 min. These parameters resulted in a density index DI = 0.14% and H_2 = 0.04 dm^3/100 g of Al-Si alloy. This is a favorable result compared to undegassed alloy, where DI = 2.18%; and H_2 = 0.16 dm^3/100 g. It has also been demonstrated that effective degassing leads to a reduction in gas porosity in the tested alloy. Crystallization studies using TDA method have shown that degassing prolongs the crystallization and, to the greatest extent, prolongs the crystallization time of the binary eutectic mixture α_{Al}+β(Si). This time, described as "τK – τB," amounted to 231 s. for undegassed alloy. Combined degassing,

carried out for parameters Z_{deg} = 1.0% and τ_{deg} = 15 min, in the case of alloy blowing with argon, prolonged the crystallization of binary eutectic mixture to 265 s, and in the case of nitrogen-degassing, to approximately 250 s. The above considerations show that degassing reduces the gas content in Al-Si alloy, while extending its crystallization time. Based on the results obtained in this study, an attempt was made to find a correlation between the level of alloy gasification and the crystallization time of the binary eutectic mixture α_{Al}+β(Si). In this case, density index DI was used to define the level of gasification. The results obtained for both series of tests are presented in Figures 10 and 11.

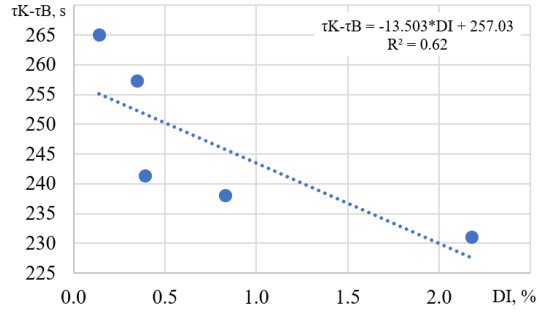

Fig. 10. The dependence of "τK – τB" crystallization time of binary eutectic mixture on the density index for Ar-degassed alloys

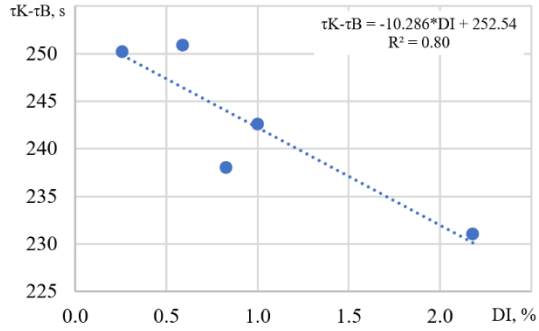

Fig. 11. The dependence of "τK – τB" crystallization time of binary eutectic mixture on the density index for N_2-degassed alloys

The data presented shows that for both test series there is a visible trend indicating the interdependence of the analyzed variables, i.e., DI index and the binary eutectic crystallization time "τK – τB" of the tested alloy. In both cases, the values of the coefficient of determination are not particularly high: for Ar-degassed alloys R^2 = 0.62, while for N_2-degassed alloys, R^2 = 0.80. However, in both research series, the volatility trend indicates an increase in the crystallization time of binary eutectic mixture along with a decrease in the level of gas content. This situation can be explained as follows. It is well known that during the degassing process, solid impurities are removed from the liquid alloy in addition to hydrogen. From the point of view of the Al-Si alloy crystallization, as well as most metallic materials, solid particles in liquid metal have a significant effect on the crystallization process [25-27]. Due to the similarity between the crystal lattice of solid inclusions and potential crystallization nuclei in the phase alloy, solid inclusions can serve as a substrate for heterogeneous nucleation of alloy component phases, i.e., phase crystallization substrate. In the case of Al-Si alloys, crystallization substrates, in particular aluminum-silicon eutectic mixture, most often consist of fine particles of previously crystallized AlP intermetallic phases and phases from the Al-Fe-Si system, as well as fine particles of the Al_2O_3 oxide layer that forms intensively on the surface of Al alloys; as well as arsenic, sulfur, selenium, and tellurium [25-30]. It can also be assumed that strong degassing may also result in more effective purification of the alloy from solid inclusions, including those that may constitute substrates for heterogeneous nucleation of alloy component phases. In view of the above, it can be reasonably assumed that an effective degassing process, accompanied by the depletion of solid phases that could serve as nucleation substrates for aluminum-silicon eutectic crystallization, leads to an extension of the crystallization time of the binary eutectic αAl+β(Si) and the alloy.

Regarding the potential application of the results in production conditions, it should be noted that the studies were conducted in laboratory conditions. Both the capacity of the furnace used for melting and degassing Al-Si alloy and the size of the test casting (TDA probe) were relatively small. The described degassing process will require verification in industrial conditions. The results obtained in this work can be used as a baseline for this verification process.

5. Conclusions

The data contained in the study shows that:

1. The most favorable density index and hydrogen content were obtained when degassing with 1% Ecosal and additional blowing with argon for 15 minutes.
2. Argon proved to be more effective as gas degasser; blowing with this gas at the same process parameters resulted in greater degassing compared to nitrogen.
3. A decrease in the density index causes an increase in "τK – τB" crystallization time of α_{Al}+β(Si) binary eutectic mixture. The probable cause of this correlation is the removal of small solid particles from the liquid metal during degassing, which could serve as a substrate for heterogeneous nucleation of the alloy components.
4. Proper degassing process reduces the porosity of the casting.

Acknowledgements

The paper was carried out as part of research project No. POIR.04.01.04-00-0117/18-00 entitled "Innovative production line for high pressure die casting with significantly reduced porosity."

References

[1] Michalek, K., Tkadlecková, M., Socha, L., Gryc, K., Saternus, M., Pieprzyca, J. & Merder, T. (2018). Physical modelling of degassing process by blowing of inert gas. *Archives of Metallurgy and Materials.* 63(2), 987-992. DOI: 10.24425/122432.

[2] Pietrowski, S. (2001). *Al-Si alloys*. Łódź: Lodz University of Technology Publishing House. (in Polish).
[3] Zhao, L., Pan, Y., Liao, H., Wang, Q. (2012). Degassing of aluminum alloys during re-melting. *Materials Letters*. 66(1), 328-331. https://doi.org/10.1016/j.matlet.2011.09.012.
[4] Samuel, A.M. & Samuel, F.H. (1992). Review. Various aspects involved in the production of low-hydrogen aluminium castings. *Journal of Materials Science*. 27(24), 6533-6563. https://doi.org/10.1007/BF01165936.
[5] Puga, H., Barbosa, J., Seabra, E., Ribeiro, S., Prokic, M. (2009). New trends in aluminium degassing—A comparative study. In Proceedings of the Fourth International Conference on Advances and Trends in Engineering Materials and Their Applications, 1-4 September 2009 (pp. 1-5). Hamburg, Germany.
[6] Eskin, D., Alba-Baena, N., Pabel, T. & da Silva, M. (2015). Ultrasonic degassing of aluminium alloys: Basic studies and practical implementation. *Materials Science and Technology.* 31(1), 79-84. https://doi.org/10.1179/1743284714Y.000000058.
[7] Puga, H., Barbosa, J., Gabriel, J., Seabra, E., Ribeiro, S. & Prokic, M. (2011). Evaluation of ultrasonic aluminium degassing by piezoelectric sensor. *Journal of Materials Processing Technology.* 211(6), 1026-1033. https://doi.org/10.1016/j.jmatprotec.2011.01.003.
[8] Abramov, V.O., Abramova, A.V., Bayazitov, V.M., Nikonov, R.V. & Cravotto, G. (2021). Pores-free aluminium alloy by efficient degassing ultrasonic treatments. *Applied Acoustics.* 184, 108343, 1-12. https://doi.org/10.1016/j.apacoust.2021.108343.
[9] Ren,Y., Chen, H., Ma, W., Lei, Y. & Zeng, Y. (2021). Purification of aluminium-silicon alloy by electromagnetic directional solidification: Degassing and grain refinement. *Separation and Purification Technology.* 277, 119459, 1-8. https://doi.org/10.1016/j.seppur.2021.119459.
[10] Rundquist, V., Paci, M. & Von Gal, R. (2019). The Development of an ultrasonic degassing process for aluminium casting. *Materials Today: Proceedings.* 10(2), 288-295. https://doi.org/10.1016/j.matpr.2018.10.408.
[11] Alba-Baena, N., Eskin, D. (2016). Kinetics of ultrasonic degassing of aluminum alloys. In Sadler, B.A. (Eds), *Light Metals 2013. The Minerals, Metals & Materials Series* (pp. 957-962). Springer, Cham. doi.org/10.1007/978-3-319-65136-1_162.
[12] Xu, H., Meek, T.T. & Han, Q. (2007). Effects of ultrasonic field and vacuum on degassing of molten aluminum alloy. *Materials Letters.* 61(4-5), 1246-1250. https://doi.org/10.1016/j.matlet.2006.07.012.
[13] Lazaro-Nebreda, J., Patel, J.B. & Fan, Z. (2021). Improved degassing efficiency and mechanical properties of A356 aluminium alloy castings by high shear melt conditioning (HSMC) technology. *Journal of Materials Processing Technology.* 294, 117146. https://doi.org/10.1016/j.jmatprotec.2021.117146.
[14] Popescu, G., Gheorghe, I., Dănilă, F. & Petru, M. (1996). Vacuum degassing of aluminum alloys. *Materials Science Forum.* 217-222, 147-152.
[15] Reddy, B.M., Nallusamy, T. (2021). Degassing of Aluminum Metals and Its Alloys in Non-ferrous Foundry. In Kumaresan, G., Shanmugam, N.S., Dhinakaran, V. (Eds.), *Advances in Materials Research* (pp. 637-644). Springer, Singapore.
[16] Socha, L., Prášil, T., Gryc, K., Sviželová, J., Nováček, P. (2022). Physical modelling of aluminum melt degassing in low-pressure die casting conditions. In 31st International Conference on Metallurgy and Materials METAL, 18-19 May 2022 (pp. 785-791). Brno, Czech Republic.
[17] Władysiak, R. (2024). Quality control of liquid aluminium alloy using thermal imaging camera. *Archives of Foundry Engineering.* 17(1), 135-140. DOI: 10.24425/afe.2024.149261.
[18] Puga, H., Barbosa, J., Tuan, N.Q. & Silva, F. (2014). Effect of ultrasonic degassing on performance of Al-based components. *Transactions of Nonferrous Metals Society of China*. 24(11), 3459-3464. https://doi.org/10.1016/S1003-6326(14)63489-0.
[19] Shih, T. S., & Weng, K. Y. (2004). Effect of a degassing treatment on the quality of Al-7Si and A356 Melts — degassing diffusers. *Materials Transactions, The Japan Institute of Metals*, 45(6), 1852-1858. https://doi.org/10.2320/matertrans.45.1852.
[20] Aluminum Degassing Methods & Measurements, A Modern Casting Staff Report. Modern Casting.
[21] PN-EN 1706: 2011. Aluminum and aluminum alloys. Castings. Chemical composition and mechanical properties.
[22] Belov, N.A., Eskin, D.G., Aksenov, A.A. (2005). *Multicomponent Phase Diagrams. Applications for commercial aluminum alloy*. Oxford: Elsevier.
[23] Glazoff, M., V., Khvan, A. & Zolotorevsky, V.S. (2018). *Casting Aluminum Alloys. Their physical and mechanical metallurgy.* Butterworth-Heinemann.
[24] Belov, N., Aksenov, A.A., Eskin, D.G. (2002). *Iron in aluminum alloys.* London: Impurity and alloying elements. CRC Press.
[25] Szymczak, T. (2019). *The effect of Cr, Mo, V, and W on the crystallization process and mechanical properties of hypoeutectic Al-Si alloys*. Łódź: Publishing House of Technical University of Lodz. (in Polish).
[26] Pietrowski, S. (1993). *Crystallization of metallic materials.* Łódź: Publishing House of Technical University of Lodz. (in Polish).
[27] Górny, Z. (1992). *Non-ferrous metal casting alloys.* Warsaw: Scientific and Technical Publishing House. (in Polish).
[28] Shankar, S., Riddle, Y.W. & Makhlouf, M.M. (2004). Eutectic solidification of aluminum silicon alloys. *Metallurgical and Materials Transactions A*. 35(9), 3038-3043. https://doi.org/10.1007/s11661-004-0048-1.
[29] Dinnis, C.M., Dahle, A.K. & Taylor, J.A. (2005). Three-dimensional analysis of eutectic grains in hypoeutectic Al–Si alloys. *Materials Science and Engineering A*. 392(1-2), 440-448. https://doi.org/10.1016/j.msea.2004.10.037.
[30] Dahle, A.K., Nogita, K., McDonald, S.D., Dinnis, C. & Lu, L. (2005), Eutectic modification and microstructure development in Al–Si alloys. *Materials Science and Engineering A.* 413-414, 243-248. https://doi.org/10.1016/j.msea.2005.09.055